

Combined cosmogenic ^{10}Be , in situ ^{14}C and ^{36}Cl concentrations constrain Holocene history and erosion depth of Grueben glacier (CH)

Christian Wirsig¹ · Susan Ivy-Ochs¹ · Naki Akçar² · Maarten Lupker³ ·
Kristina Hippe¹ · Lukas Wacker¹ · Christof Vockenhuber¹ · Christian Schlüchter²

Received: 7 December 2015 / Accepted: 29 August 2016 / Published online: 14 September 2016
© Swiss Geological Society 2016

Abstract Surface exposure dating with a single cosmogenic nuclide relies on the assumption of simple constant exposure. In contrast, the combination of nuclides with different half-lives or production rate depth profiles allows constraining complex exposure histories. Here we present the systematics of how the combination of ^{10}Be , in situ ^{14}C and ^{36}Cl can be used to understand both burial and erosion in a rock surface, in addition to yielding an exposure time. Concordant ages of all three nuclides characterize simple exposure. Apparently ‘too young’ ^{14}C ages or ‘too old’ ^{36}Cl ages indicate burial or erosion of the rock surface, respectively. We further report a first data set from a proglacial granite bedrock ridge in a small cirque in the Central Swiss Alps. Three samples were exposed for 9.6 ± 0.3 ka during the Holocene. The use of same-sample ^{10}Be , in situ ^{14}C and ^{36}Cl allowed us to quantitatively show that these rock surfaces experienced simple constant exposure with ≤ 500 years of ice cover and ≤ 6 cm of erosion. In addition, the fact that samples inside and outside the Little Ice Age (LIA) ice extent yield indistinguishable ages reinforces the hypothesis that Grueben glacier reached comparable dimensions only briefly during the Holocene. Notably, at sites just inside of the LIA

extent, which do exhibit fresh glacial polish, concordant ages suggest that subglacial erosion there was minimal.

Keywords Cosmogenic nuclides · Oberhasli · Grimsel · In situ ^{14}C · Holocene glacier history · Subglacial erosion

1 Introduction

The concentration of cosmogenic nuclides in rocks is used by geomorphologists to gain knowledge on the age of landforms such as moraines or landslides (Gosse and Phillips 2001; Bierman et al. 2002; Ivy-Ochs and Kober 2008). In many studies, considerations based on geomorphological field evidence allow the assumption that rock surfaces were exposed in a single continuous episode. Then the analysis of one cosmogenic nuclide species suffices for dating purposes. This assumption is violated, however, if temporary burial or erosion of the rock surface cannot be excluded. In these cases, the combination of multiple cosmogenic nuclides can potentially resolve the details of the landform history (Miller et al. 2006). Indeed, the complexity itself is often the subject of interest: how long was a surface covered by ice or sediment? How deep was the bedrock underneath a glacier eroded? Whereas in the past, mainly the pair of ^{10}Be and ^{26}Al has been utilized successfully to unravel complex exposure histories (Bierman et al. 1999; Corbett et al. 2013), in this study we combine same-sample results from ^{10}Be , in situ ^{14}C and ^{36}Cl .

The system of ^{10}Be is the most frequently used and best understood amongst all cosmogenic nuclides. It has proven to be a reliable dating method on a broad temporal scale from centuries (Schimmelpennig et al. 2014) to millions of years (Ivy-Ochs et al. 1995). In situ ^{14}C has the potential to

Editorial handling: E. Gnos.

✉ Susan Ivy-Ochs
ivy@phys.ethz.ch

¹ Laboratory of Ion Beam Physics, ETH Zürich, Otto-Stern-Weg 5, 8093 Zurich, Switzerland

² Institute of Geological Sciences, University of Bern, Baltzerstrasse 1 + 3, 3012 Bern, Switzerland

³ Institute of Geochemistry and Petrology, ETH Zürich, Clausiusstrasse 25, 8092 Zurich, Switzerland

add substantial information about recent episodes of burial. Compared to ^{26}Al it decays more rapidly ($t_{1/2} = 5.7$ ka) and can thus allow detection of shorter burial periods down to a few centuries (Miller et al. 2006; Goehring et al. 2011; Hippe et al. 2012). Owing to the challenges in the extraction process of in situ ^{14}C from quartz mineral separates (Lifton et al. 2001), only a few studies employing this nuclide have been reported. Both nuclides, ^{10}Be and in situ ^{14}C , are mainly produced by spallation reactions from high-energy neutrons with secondary contributions from muon interactions. ^{36}Cl , in contrast, is produced in a variety of pathways depending on the chemistry of the host rock (Gosse and Phillips 2001; Alfimov and Ivy-Ochs 2009). In particular, capture of thermal neutrons by ^{35}Cl can contribute significantly to the production of ^{36}Cl . A part of the thermal neutrons are lost close to the rock surface due to diffusion (Fabryka-Martin 1988; Phillips et al. 2001). Therefore, ^{36}Cl production in rocks typically peaks at a depth of a few decimeters (depending on the concentration of natural chlorine), not at the rock surface (cf. Figure 1). When analyses of ^{36}Cl and ^{10}Be or ^{14}C are combined, the difference in the shape of their production rate depth profiles can be used to quantify the depth of erosion.

The following three scenarios serve to illustrate how combined analyses of ^{10}Be , ^{14}C and ^{36}Cl can allow distinguishing between constant exposure, burial and erosion scenarios (Figs. 2, 3). (a) In a scenario with one continuous period $t_e = 9.6$ ka of exposure (Fig. 2, solid lines), cosmogenic nuclides form constantly and decay according to the different half-lives. The final concentrations of each nuclide correspond to an exposure age of 9.6 ka (Fig. 3a). Concordant ages (within uncertainties) calculated from all

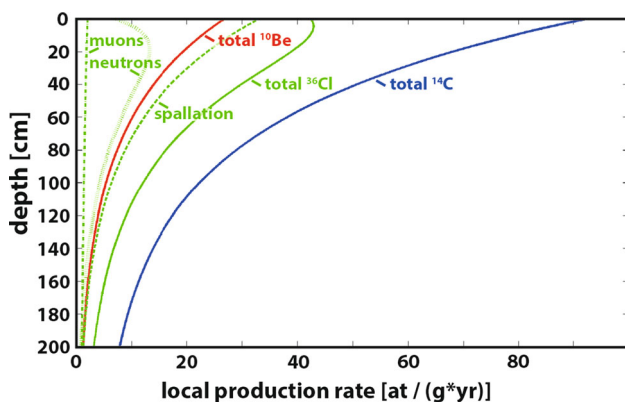


Fig. 1 Modelled production rate depth profile for sample Grub2, see chemical composition in Table 3. Solid lines are total production rates for ^{10}Be (red), ^{14}C (blue) and ^{36}Cl (green). Detailed contribution of different production pathways are shown for ^{36}Cl . The magnitude of the characteristic subsurface production peak caused by thermal and epithermal neutrons (dotted line) depends on the concentration of ^{35}Cl in the rock

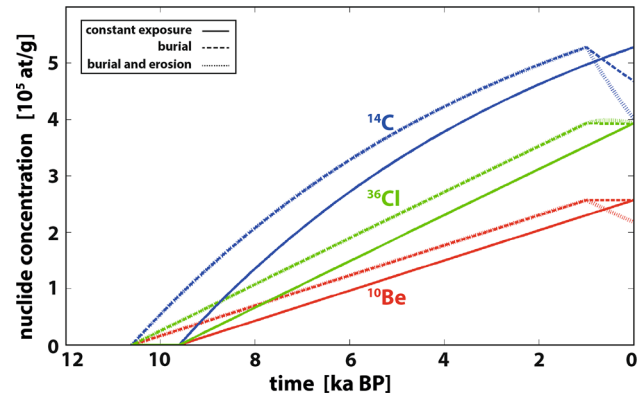


Fig. 2 Modelled evolution of ^{10}Be (red), ^{14}C (blue) and ^{36}Cl (green) nuclide concentrations in sample Grub2 for three different scenarios. **a** Solid constant exposure for 9.6 ka. **b** Dashed 9.6 ka exposure followed by 1.0 ka burial. **c** Dotted same as **b**, but total erosion of 10 cm during the period of burial, equivalent to a subglacial erosion rate of 0.1 mm/a

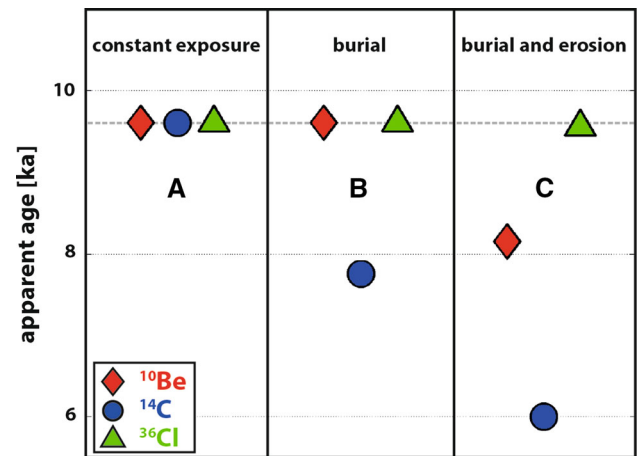


Fig. 3 Apparent exposure ages calculated from the final nuclide concentrations of the scenarios described in Fig. 2. The constant exposure scenario (a) yields identical exposure ages from each nuclide. The burial scenarios with or without erosion (b, c) are characterized by systematic deviations in apparent ages: compared to ^{10}Be , ‘too low’ ^{14}C ages indicate burial periods, ‘too high’ ^{36}Cl ages point to erosion of the rock surface

measured nuclides therefore indicate constant exposure. (b) If after the exposure period the samples were temporarily covered and shielded from cosmic radiation, for example by a glacier for a duration of $t_b = 1.0$ ka (Fig. 2, dashed lines), no new nuclides are produced during that episode whilst radioactive decay continues. Due to their long half-lives, ^{10}Be and ^{36}Cl experience only negligible decay while the concentration of ^{14}C drops significantly because of its comparably short half-life. Apparently too young ^{14}C ages (compared to ^{10}Be and ^{36}Cl) therefore characterize burial (Fig. 3b). (c) Additionally, the samples could be affected by an erosion rate of 0.1 mm/a during the period of burial (‘subglacial erosion’, dotted lines in Fig. 2). Due to the

above-mentioned subsurface production peak the concentration of previously accumulated ^{36}Cl slightly increases in the first decimeters below the rock surface (Fig. 1). Erosion causes the rock surface to approach the peak. Hence the concentrations of ^{10}Be and ^{14}C decrease more rapidly than ^{36}Cl concentrations and apparently too old ^{36}Cl ages (compared to ^{10}Be and ^{14}C) indicate erosion. Conflicting apparent exposure ages with $t_{36} > t_{10} > t_{14}$ therefore characterize the burial and erosion scenario (Fig. 3c).

In the following we present a pilot study combining same-sample ^{10}Be , ^{14}C and ^{36}Cl analyses. In a simple deglaciation setting in a well-mapped study area, the aim is to gain knowledge on the dimensions of a cirque glacier in the Alps throughout the Holocene. How long was the glacier as extensive as during the LIA, or even more extensive? How deeply did the glacier erode the bedrock? The multi-nuclide approach was chosen as a tool with the theoretical capability to address these questions. Parts of the proposed method have been employed in several studies to detect either burial or erosion (e.g. Fabel et al. 2004; Goehring et al. 2011), but never before in this combination to constrain both simultaneously.

2 Setting

Gruebengletscher is a relatively small cirque glacier in a tributary valley to the Haslital close to Grimsel Pass in the central part of the Swiss Alps (Fig. 4). The surrounding area is characterized by widespread granite lithologies, in our study area mostly Central Aare granite crosscut by a band of metamorphic units ('Altkristallin'; Abrecht 1994). These weathering resistant rocks display well-preserved glacial landscape elements such as U-shaped trough valleys and roche moutonnées. During the Last Glacial Maximum (LGM) the Grueben cirque was filled with more than 500 m of ice that was connected to the Aare Glacier, which extended out into the Swiss Alpine Foreland (Florineth and Schlüchter 1998; Bini et al. 2009; Wirsig et al. 2016). Due to its high elevation above 1700 m it can be assumed that it was occupied by glaciers throughout the Lateglacial period until the end of the Younger Dryas cold spell at 11.5 ka (Maisch et al. 1999). Glacier sizes during most of the Holocene were probably confined to within the well-documented maximum extent of the Little Ice Age (LIA) glacier re-advance (Swisstopo 1865; Maisch et al. 1999; Ivy-Ochs

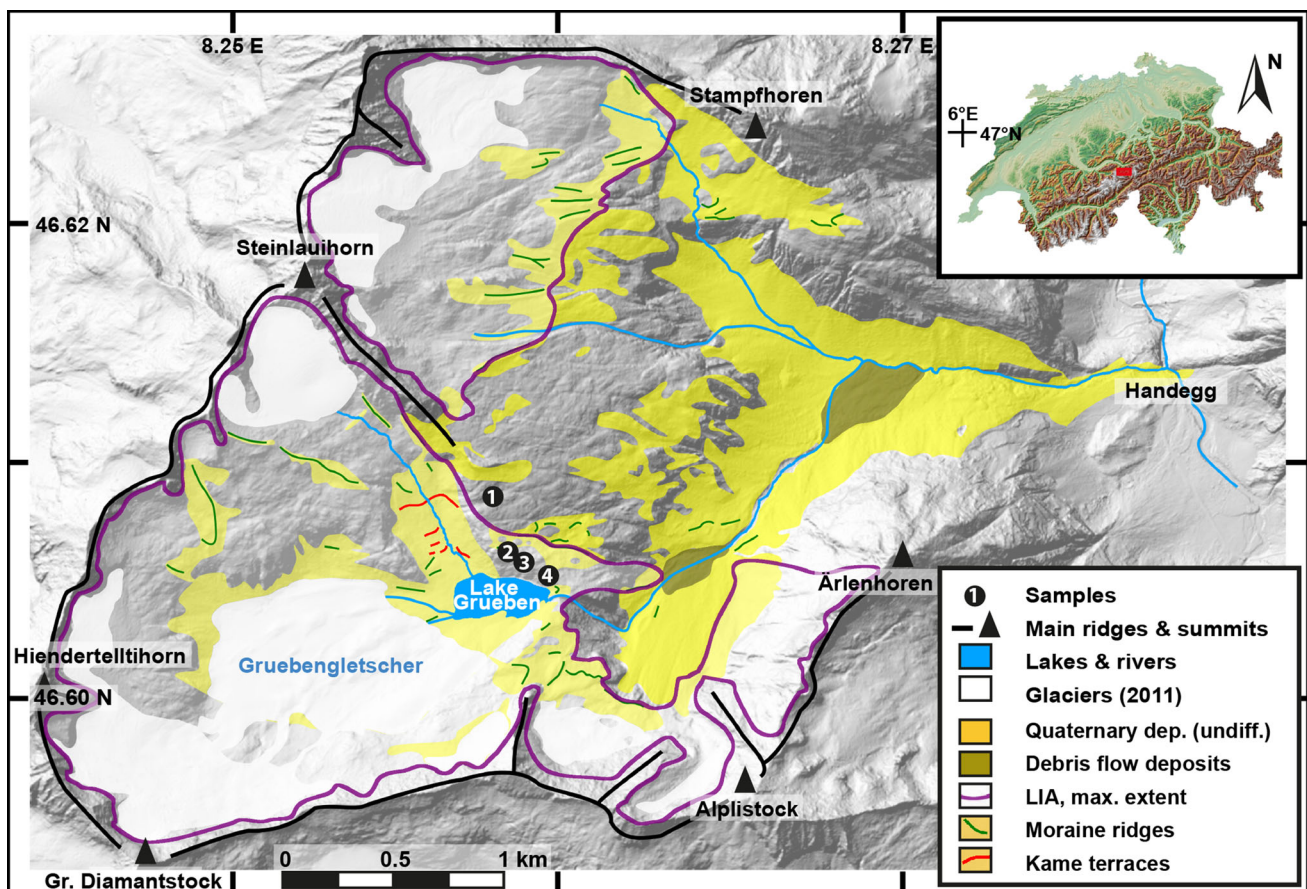


Fig. 4 Map of the study area including the four sampling sites (modified from Kämpfer (2012)) with a hill-shade model in the background [reproduced by permission of swisstopo (JA100120)].

The red square in the inset in the upper right corner indicates the location of the area within Switzerland

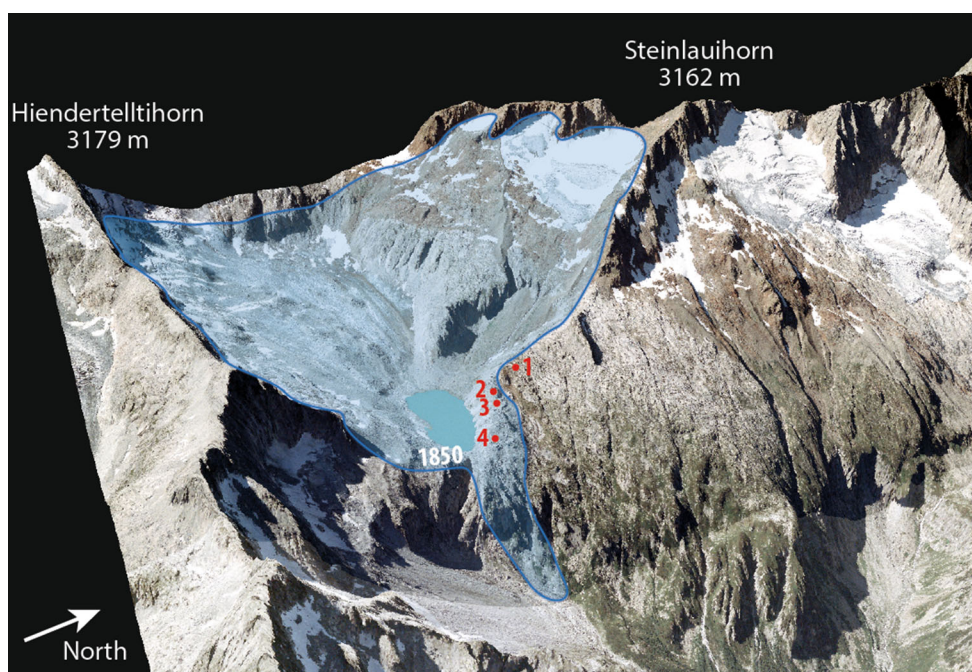


Fig. 5 3D-model of the study area including the four sampling sites and the footprint of Grueben glacier at ~1850 (Swisstopo 1865). Grub2-4 were covered by Grueben glacier during the LIA, Grub1 not.

The model is based on swissALTI3D DEM and Landsat images used with permission of swisstopo (JA100120)

et al. 2009), even though a few moraine ridges are preserved outside of this perimeter (see Figs. 4, 5). Bedrock that was covered by ice during the LIA is clearly discernible based on its fresh appearance in comparison to bedrock outside this extent that is significantly more weathered and covered with lichen. Since deglaciation, slope processes such as rock falls and debris flows constituted a major impact on the Grueben valley. Kame terraces on the NW-slope above Lake Grueben indicate the approximate ice levels in the first half of the twentieth century (see Fig. 4; Kämpfer 2012; Kämpfer and Hählen 2014).

Four samples were collected from the bedrock ridge that rises almost vertically for more than 100 m to the north of Lake Grueben (Fig. 5). Due to its orientation parallel to the general valley slope, Holocene glaciers were directed down-valley by this wall of bedrock. Presumably, only at the largest Holocene glacier extents, such as the LIA, did significant amounts of ice cross over this ridge. The bedrock samples were taken along the ridge crest, one outside (Grub1) and three inside (Grub2-4) the maximum LIA extent forming a transect with decreasing elevation from 2465 to 2374 m. The sampled bedrock within the LIA extent is smooth and glacially polished. The conserved glacial polish on the rock surface indicates negligible erosion in the absence of ice. Outside of the LIA, the ridge also exhibits clear signs of glacial moulding. However, a surface roughness of approximately 1 cm (i.e. protruding quartz grains) indicates a somewhat higher degree of weathering.

3 Methods

Less than 3 cm thick pieces of bedrock were gathered using hammer and chisel. In order to minimize the influence of temporary cover by sediment or snow, samples were collected at carefully chosen spots on the top of prominent roche moutonnée features. Locations on the abrasion side were preferred and areas affected by plucking avoided. Grub4 originates not from the highest point of a roche moutonnée, but near to a small depression.

The material was crushed and sieved to grain sizes of $<800 \mu\text{m}$ for Be and C and $88 \mu\text{m} < \text{grain size} < 500 \mu\text{m}$ for Cl aliquots. Be sample preparation from quartz mineral separates is based on the method of Kohl and Nishiizumi (1992) with some modifications (Ivy-Ochs et al. 2006). The $^{10}\text{Be}/^9\text{Be}$ ratio was measured on the 6 MV TANDEM AMS facility (Kubik and Christl 2010; Christl et al. 2013) at the Laboratory of Ion Beam Physics (LIP) at ETH Zürich relative to the 07KNSTD standard (Nishiizumi et al. 2007). The reported values are corrected for a long-term average full process blank ratio of $(3.6 \pm 2.6) \times 10^{-15} \text{ }^{10}\text{Be}/^9\text{Be}$. *In situ* ^{14}C was extracted from $\sim 5 \text{ g}$ of quartz mineral separates following the procedures outlined in Hippe et al. (2009, 2013). Samples were then measured at the LIP on a MICADAS AMS system equipped with a gas ion source (Fahrni et al. 2013; Wacker et al. 2013). Data analysis follows Hippe et al. (2013) using a long-term average blank value of $(3.0 \pm 1.4) \times 10^4 \text{ }^{14}\text{C}$ atoms based on 20

measurements in the same year. Chlorine was separated from whole rock (Aare granite) samples following the methods published by Zreda (1994) and Stone et al. (1996) with modifications by Ivy-Ochs (1996) using a ^{35}Cl -enriched spike provided by Oak Ridge National Laboratory for isotope dilution (Ivy-Ochs et al. 2004). ^{36}Cl AMS and stable Cl measurements were conducted at the LIP TANDEM system at ETH Zürich relative to the internal K382/4 N standard (Christl et al. 2013). A user blank correction of $^{36}\text{Cl}/^{35}\text{Cl} = 3.4 \times 10^{-15}$ was applied. The chemical composition was determined by SGS in Ontario, Canada with XRF and ICP techniques.

The CRONUS-EARTH online calculator (Balco et al. 2008) was used to calculate ^{10}Be exposure ages with a spallogenic production rate at SLHL of 3.93 ± 0.19 at/g/a ('NENA', 'St' scaling; Balco et al. 2009). For in situ ^{14}C , ages are based on a spallogenic production rate at SLHL of 12.3 ± 0.5 at/g/a ('St' scaling; Young et al. 2014). Contributions from muogenic production pathways were modelled in MATLAB with the code from Balco et al. (2008) based on the methods of Heisinger et al. (2002a, b). ^{36}Cl exposure ages were calculated by a MATLAB model implementing the equations and constants presented in Alfimov and Ivy-Ochs (2009), in particular spallogenic production rates (without muons) at SLHL of 48.8 ± 3.4 at/g/a for Ca (Stone et al. 1996) and 162 ± 24 at/g/a for K (Evans et al. 1997). These values agree well within errors with recently published production rates (Borchers et al. 2016; Marrero et al. 2016).

The stated age uncertainties (1σ) include AMS standard reproducibility, counting statistics, standard mean error of

samples and the propagation of input uncertainties, in particular of the production rate and the 'St' scaling scheme of Lal (1991) and Stone (2000). For in situ ^{14}C , the reproducibility of the extraction system contributes an additional uncertainty of 5%. 'Apparent ages' are the theoretical ages calculated from nuclide concentrations in a simple exposure scenario with no erosion. We use them here as a more accessible representation of nuclide concentrations. They do not define a true exposure age of a rock surface, as long as its burial and erosion history are unclear.

4 Results

Sample information and measured cosmogenic nuclide concentrations are listed in Table 1. All three nuclides were successfully measured in Grub2-4. Grub1 yielded results for ^{10}Be as well as ^{14}C , but not ^{36}Cl due to lack of sufficient sample material. Additional data on the ^{14}C measurements are reported in Table 2. The chemical compositions of Grub2-4 are presented in Table 3. Natural chlorine is present in all samples at relatively low levels of 21.6–31.7 ppm. Finally, Table 4 summarizes calculated apparent exposure ages and uncertainties at the 1σ level. The obtained apparent exposure ages range from 7.4 ± 0.4 to 10.6 ± 0.8 ka. They are graphically summarized in Fig. 6. For each individual sample, the ages derived from different nuclides agree within the 2σ uncertainty range. The average apparent exposure ages (arithmetic mean) of Grub1, Grub2 and Grub3 are indistinguishable at 9.5–9.9 ka with ~ 0.7 ka uncertainty (1σ). Grub4 appears

Table 1 List of samples, basic parameters and measured cosmogenic nuclide concentrations

Sample ID	Latitude (WGS 84)	Longitude (WGS 84)	Elevation (m a.s.l.)	Thickness (cm)	topographic shielding	^{10}Be conc. (10^5 at/g _{qtz} ^a)	^{14}C conc. (10^5 at/g _{qtz})	^{36}Cl conc. (10^5 at/g _{sample} ^b)
Grub1	46.607	8.266	2465	1.0	0.99	2.88 ± 0.10	5.22 ± 0.26	
Grub2	46.606	8.267	2416	1.0	0.99	2.21 ± 0.12	5.17 ± 0.26	4.52 ± 0.27
Grub3	46.605	8.268	2405	2.0	0.99	2.69 ± 0.15	5.20 ± 0.26	3.45 ± 0.24
Grub4	46.605	8.269	2374	3.0	0.99	2.03 ± 0.11	4.29 ± 0.21	3.92 ± 0.21

^a Measured against standard 07KNSTD (Nishiizumi et al. 2007), corrected for full process blank of $(3.6 \pm 2.6) \times 10^{-15}$ $^{10}\text{Be}/^9\text{Be}$

^b Measured against standard K382/4N (Christl et al. 2013), corrected for full process blank of 3.4×10^{-15} $^{36}\text{Cl}/^{35}\text{Cl}$

Table 2 Additional ^{14}C data

Sample ID	AMS ID	Sample mass (g)	CO ₂ yield (μg)	Fraction modern ($F^{14}\text{C}$) ^a	$\delta^{13}\text{C}$ (‰)	$^{14}\text{C}/^{12}\text{C}$ abs (10^{-12}) ^b
Grub1	47404.1.1	4.92	6.4	6.88 ± 0.06	-22.0	8.16 ± 0.07
Grub2	46388.1.1	4.74	9.7	4.33 ± 0.04	-20.2	5.16 ± 0.05
Grub3	47405.1.1	4.50	3.5	11.57 ± 0.10	-25.4	13.64 ± 0.12
Grub4	47408.1.1	5.07	5.9	6.45 ± 0.06	-31.1	7.53 ± 0.07

^a Normalized to $\delta^{13}\text{C}$ of -25 ‰ VPDB and AD 1950

^b Calculated after Eq. 1 in (Hippe et al. 2013) using a blank of $(3.0 \pm 1.4) \times 10^4$ ^{14}C atoms

Table 3 Elemental composition of samples analyzed for ^{36}Cl

Sample ID	Al_2O_3 (%)	CaO (%)	Cr_2O_3 (%)	Fe_2O_3 (%)	K_2O (%)	MgO (%)	MnO (%)	Na_2O (%)	P_2O_5 (%)	SiO_2 (%)	TiO_2 (%)	Sm (ppm)	Gd (ppm)	U (ppm)	Th (ppm)	Cl (ppm)
Grub2	9.91	1.25	0.005	1.08	3.44	0.22	0.03	3.00	0.02	75.70	0.10	5.9	6.1	9.7	34.4	31.7 ± 0.5
Grub3	10.4	1.14	0.005	1.30	3.39	0.15	0.05	3.30	0.02	75.70	0.10	4.8	4.8	7.9	22.7	21.6 ± 0.2
Grub4	11.2	0.82	0.005	1.40	4.00	0.14	0.04	3.20	0.01	75.40	0.11	5.9	5.3	8.0	28.3	26.2 ± 0.1

to be slightly younger with a mean apparent age of 8.1 ± 0.5 ka.

If the bedrock surfaces are assumed to have been covered by 100 cm of seasonal snow (0.3 g/cm^3) for 6 months per year (Hippe et al. 2014), the mean ages increase to 10.8–11.2 ka for Grub1-3 and 9.2 ± 0.5 ka for Grub4 (Gosse and Phillips 2001). The discussion is based on the apparent ages without snow shielding, as the average amount of seasonal snow cover during the entire Holocene is not known. Snow cover does not affect the conclusions drawn here.

5 Discussion

The analysis of multiple cosmogenic nuclide concentrations enables us to understand exposure duration, cover duration, and erosion depth of the sampled rock surfaces. The key to the interpretation is in the relation between the apparent ages derived from the different nuclides. As illustrated above, the measured nuclide ratios characterize a certain type of exposure history (Figs. 2, 3). The production systematics and decay constants of the individual nuclides allow systematic deviations only in one direction, however: same-sample apparent ^{14}C ages can only be younger than or equal to apparent ^{10}Be or ^{36}Cl ages. Likewise, given the elemental composition of our samples, apparent ^{36}Cl ages can only be older than or equal to apparent ^{10}Be or ^{14}C ages. In this study, however, the different nuclides appear in a random order, i.e. in some cases ^{10}Be ages are slightly older than ^{14}C or ^{36}Cl ages, sometimes younger. Since for each sample the apparent ages of the three analyzed nuclides agree with that sample's mean age within 2σ uncertainty (seven of eleven ages within 1σ), this strongly indicates that there is no systematic deviation from concordant nuclide ages in our data set. The spread in individual nuclide ages thus represents the expected statistical distribution given the uncertainty of individual measurements and age calculations. The concordant same-sample ages imply that the rock surfaces were constantly exposed (see Figs. 2, 3). The influence of burial and erosion was too small to manifest in offsets of cosmogenic nuclide concentrations. In this simple exposure setting, the calculated 'apparent ages' can therefore be considered as true exposure ages of the rock surfaces.

Simple exposure and/or known inheritance is one of the major assumptions of surface exposure dating. Here, the combination of different cosmogenic nuclides allows us to test this assumption and eventually infer that this is actually the case. Essentially, they enable us to formulate constraints: how long could a cover period be without being detected?—i.e., what is the minimum duration of cover that leads to significant differences in apparent ages

Table 4 Calculated apparent surface exposure ages and uncertainties (1σ)

Sample ID	^{10}Be age ^a (ka)	^{14}C age ^b (ka)	^{36}Cl age ^c (ka)	Mean age (ka)
Grub1	10.6 ± 0.6	9.2 ± 0.5		9.9 ± 0.7
Grub2	8.3 ± 0.6	9.5 ± 0.5	10.6 ± 0.8	9.5 ± 0.7
Grub3	10.3 ± 0.7	9.8 ± 0.5	8.8 ± 0.7	9.6 ± 0.4
Grub4	8.0 ± 0.6	7.4 ± 0.4	8.9 ± 0.6	8.1 ± 0.5

^a Using NENA production rates (Balco et al. 2009). For all nuclides ‘St’ scaling, zero erosion and a rock density of 2.65 g/cm^3 are assumed

^b Using a spallogenic production rate at SLHL of $(12.3 \pm 0.5) \text{ at/g/a}$ (Young et al. 2014)

^c Using spallogenic production rates at SLHL of $(48.8 \pm 3.4) \text{ at/g/(Ca)}$ (Stone et al. 1996) and $(162 \pm 24) \text{ at/g/a (K)}$ (Evans et al. 1997)

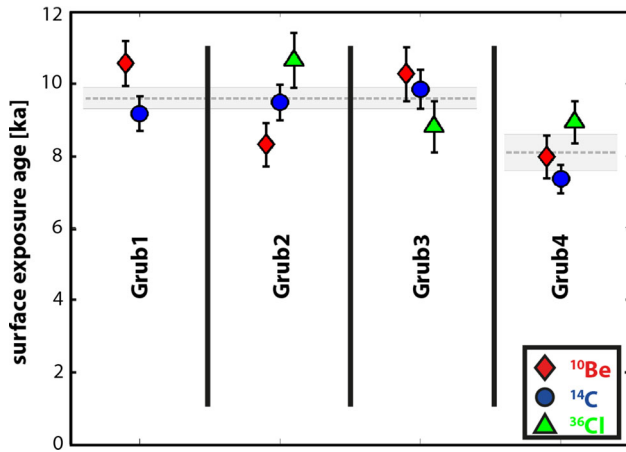


Fig. 6 Comparison of apparent surface exposure ages and uncertainties (1σ) calculated from ^{10}Be , ^{14}C and ^{36}Cl concentrations. The dashed grey line and surrounding area mark the mean age and uncertainty of samples Grub1-3 of 9.6 ± 0.3 and of 8.1 ± 0.5 ka for Grub4, respectively. All nuclide ages agree with the corresponding mean age when the 2σ -uncertainty interval is considered

of the individual nuclides? Likewise, how deep can the rock surfaces have been eroded before we expect to detect it? Numerical modelling of scenarios with varying exposure histories provides insight into the sensitivity of the method. The influence of the duration of burial on apparent ages is investigated in Fig. 7a. It shows apparent ages that result from 9.6 ka exposure followed by varying durations of burial (glacial cover) as predicted by hundreds of model runs. The longer the cover, the more the apparent ^{14}C ages deviate from apparent ^{10}Be and ^{36}Cl ages. The arithmetic mean of errors of individual nuclide ages is $\sim 6\%$ (1σ). This propagates to $\sim 8.5\%$ uncertainty on age ratios. According to Fig. 7a apparent ^{14}C ages would deviate from ^{10}Be and ^{36}Cl significantly ($>8.5\%$) if the rock surface had been covered for more than ~ 500 years.

The sensitivity of apparent ages to the depth of erosion is portrayed in Fig. 7b. It shows apparent ages that result from 9.6 ka exposure followed by 500 years of glacial cover. The erosion depth occurring during the cover is varied from 0 to 15 cm. The deeper the erosion, the more

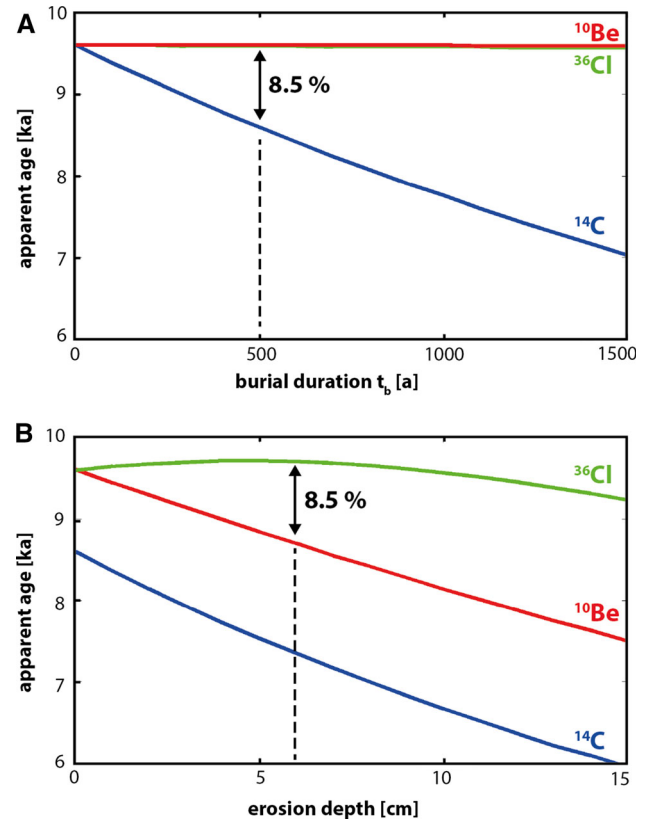


Fig. 7 Sensitivity to burial and erosion. Apparent exposure ages of Grub2 calculated for two sets of scenarios. Concentration uncertainties of 6% , resulting in 8.5% uncertainties on nuclide ratios, are used for sensitivity statements. **A** 9.6 ka of exposure followed by a burial period of $t_b = 0$ –1500 years. $t_b = 1000$ years is identical to scenario **B** in Figs. 2 and 3. If burial lasts longer than ~ 500 years, in situ ^{14}C is expected to yield significantly lower apparent ages than ^{10}Be or ^{36}Cl . **B** 9.6 ka of exposure followed by a burial period of 500 years. While buried, the surface is eroded by 0–15 cm by glacial erosion. The starting point at erosion depth = 0 is the same as $t_b = 500$ years in panel A. If more than ~ 6 cm are eroded, ^{36}Cl yields significantly higher apparent ages than ^{10}Be

^{36}Cl ages appear older than ^{10}Be ages. Following the same reasoning as above, our uncertainties allow detection of age deviations if they are greater than $\sim 8.5\%$. The minimum erosion depth we expect to detect therefore is ~ 6 cm

(Fig. 7b). This converts to a subglacial erosion rate of 0.12 mm/a, if the site had been covered for e.g. 500 years. Taken together, the concordant ages of the three nuclides on each sample imply that our samples were covered for less than 500 years and eroded by less than 6 cm. There was effectively no erosion and only very brief ice cover at the lateral margin of the LIA Grueben glacier.

These conclusions are reinforced when the sample locations relative to the LIA ice margin are taken into consideration (Fig. 5). Despite the fact that Grub2 and Grub3 were covered by ice during the LIA advance, while Grub1 was not, the three samples yield indistinguishable mean ages. This leads to two main implications. First, during the Holocene, Grueben glacier grew to dimensions similar to the maximum LIA extent only briefly, i.e. too short for the ice cover to cause younger ^{14}C ages in Grub2 and Grub3. Assuming that no nuclides were inherited from exposure periods before the Younger Dryas (e.g. Ivy-Ochs et al. 2007), then Grueben glacier was smaller than its maximum LIA extent for more than 9.6 ± 0.3 ka during the Holocene. This is in excellent agreement with data from other sites that suggest that glaciers in the Alps are considered to have been smaller than today for most of the Holocene (Holzhauser et al. 2005; Joerin et al. 2006; Ivy-Ochs et al. 2009; Goehring et al. 2011). Second, the total erosion of bedrock at the lateral ice margin of the LIA Grueben glacier was negligible. Otherwise we would have observed apparently younger ages inside than outside the LIA glacier footprint. Even though the fresh glacial polish indicates that the bedrock within the LIA perimeter was moulded by the glacier, it must have been only thinly abraded rather than deeply eroded. The ubiquitous glacial erosional features encountered on the ridge were therefore formed earlier in time and not destroyed since. Similar results were first obtained by Fabel et al. (2004), demonstrating that glacial scouring near the lateral ice margins in trough valley cross sections was low despite the presence of striations. Both implications outlined here support the conclusions drawn from the multi-nuclide analysis.

The age of sample Grub4 (8.1 ± 0.5 ka) appears to be younger than the other samples, which can be explained by three scenarios. First, it could be assumed that the sample spot was exposed roughly 1.5 ka later than the others, after prolonged cover by ice or till deposited at this site by the Egesen stadial glacier, and continuously exposed since. This would result in concordant ^{10}Be , in situ ^{14}C and ^{36}Cl ages, as is actually the case when the 2σ -uncertainty interval is considered. Second, constant exposure for 9.6 ka like Grub1-3, but covered by ~ 150 cm of snow for 6 months per year would result in an apparent age of 8.1 ka for Grub4. Since snow cover also enhances the neutron flux in the rock surface (Dunai et al. 2014), ^{36}Cl ages would appear 'too old'. The comparably flat sample surface close to a local depression could serve as an

argument to support these two scenarios, even though the difference in snow depth in comparison to the other samples appears rather large. However, the relative distribution of ages with $t_{36} > t_{10} > t_{14}$ hints at the third possible interpretation: a burial and erosion scenario as illustrated in Fig. 2 (dotted lines) and Fig. 3c. Because of its lower elevation, i.e. its position 'more inside the ice', Grub4 was likely covered by glacier advances more frequently during the Holocene than the other sample spots that are almost at the limit (Grub2,3) or even beyond (Grub1) the maximum LIA extent. Consequently, the difference in apparent exposure ages could be interpreted to record the integrated time that Grueben glacier was big enough to cover Grub4, but not Grub1-3. Yet, compared to the ^{10}Be age from Grub4, the in situ ^{14}C age does not appear significantly younger and the ^{36}Cl age does not appear significantly older. As argued above, this implies that glacial coverage of Grub4 was shorter than 500 years and subglacial erosion less than 6 cm. Therefore, only a part of the ~ 1500 years age difference could be explained by late burial and erosion. Conceivably, the nuclide concentrations measured in Grub4 could result from a combination of the three scenarios described here: delayed initial exposure, snow cover and burial + erosion caused by Grueben glacier.

We expect that Grueben glacier was big enough to cover and erode the bedrock at lower elevations and proximity to Lake Grueben more often during the Holocene. This should lead to generally younger apparent ages if our transect were extended downhill. Additionally, the mismatch between apparent ages calculated from ^{10}Be , in situ ^{14}C and ^{36}Cl would increase. Similar observations were initially made along a profile on proglacial bedrock at the nearby Rhône glacier with the ^{10}Be and in situ ^{14}C nuclide pair (Goehring et al. 2011).

6 Conclusions

Two independent lines of arguments were provided to address the major objective of this study; to gain information on the size of and erosion caused by an Alpine cirque glacier during the Holocene. First, concordant apparent ages for individual samples acquired by cosmogenic ^{10}Be , in situ ^{14}C and ^{36}Cl analysis imply a simple exposure history. This could be quantified by deducing that the rock surfaces were covered for less than 500 years, otherwise apparent in situ ^{14}C ages would be younger than apparent ^{10}Be and ^{36}Cl ages. Because ^{36}Cl yields identical apparent ages that are not older than ^{10}Be and in situ ^{14}C , total erosion was calculated to be less than 6 cm.

Secondly, samples Grub1-3 yield indistinguishable mean ages of 9.5–9.9 ka. Since exposure ages outside (Grub1) and within (Grub2,3) the LIA maximum glacier extent agree, Grueben glacier was rarely big enough to cover Grub2 and Grub3 and did not cause sufficient erosion

at its lateral ice margin to significantly impact the nuclide inventory in the rock. This conforms well to the results of the multi-nuclide analysis.

Grub4 appears ~ 1.5 ka younger than the other samples: 8.1 ± 0.5 ka. The difference could be caused by a combination of (a) delayed initial exposure, (b) snow cover and/or (c) burial + erosion caused by Grueben glacier. Future studies are planned to investigate if cover duration and erosion depth increase towards the center of the glacial trough (Fabel et al. 2004; Goehring et al. 2011). This is a likely possibility because Holocene glacier advances reached these positions more frequently and covered them by thicker ice than at the lateral ice margins.

Single-nuclide studies rely on the assumption of a simple exposure history and a priori estimation of local erosion rates to calculate surface exposure ages. We showed that the combination of cosmogenic ^{10}Be , in situ ^{14}C and ^{36}Cl proves to be a valuable tool to avoid or to test these assumptions. In addition to the determination of exposure ages for the sampled rock surfaces, the multi-nuclide approach enabled us to place significant constraints on the duration of temporary burial (e.g. underneath a glacier) and depth of erosion caused by the glacier.

Acknowledgements Suggestions of two anonymous reviewers and editor E. Gnos greatly improved this paper. This work was supported by the Swiss National Fonds (SNF), Project 2-77099-11. We thank P. W. Kubik for ^{10}Be measurements. We are grateful for the support of the whole team at LIP, ETHZ.

References

- Abrecht, J. (1994). Geologic units of the Aar massif and their pre-Alpine rock associations: A critical review. *Schweizerische Mineralogische und Petrographische Mitteilungen*, 74, 5–27.
- Alfimov, V., & Ivy-Ochs, S. (2009). How well do we understand production of ^{36}Cl in limestone and dolomite? *Quaternary Geochronology*, 4, 462–474.
- Balco, G., Briner, J., Finkel, R. C., Rayburn, J. A., Ridge, J. C., & Schaefer, J. M. (2009). Regional beryllium-10 production rate calibration for late-glacial northeastern North America. *Quaternary Geochronology*, 4, 93–107.
- Balco, G., Stone, J. O., Lifton, N. A., & Dunai, T. J. (2008). A complete and easily accessible means of calculating surface exposure ages or erosion rates from ^{10}Be and ^{26}Al measurements. *Quaternary Geochronology*, 3, 174–195.
- Bierman, P. R., Caffee, M. W., Davis, P. T., Marsella, K., Pavich, M., Colgan, P., et al. (2002). Rates and timing of earth surface processes from in situ-produced cosmogenic Be-10. *Reviews in Mineralogy and Geochemistry*, 50, 147–205.
- Bierman, P. R., Marsella, K. A., Patterson, C., Thompson Davis, P., & Caffee, M. (1999). Mid-Pleistocene cosmogenic minimum-age limits for pre-Wisconsinian glacial surfaces in southwestern Minnesota and southern Baffin Island: A multiple nuclide approach. *Geomorphology*, 27, 25–39.
- Bini, A., Buoncristiani, J. F., Couterrand, S., Ellwanger, D., Felber, M., Florineth, D., et al. (2009). *Switzerland during the Last Glacial Maximum 1: 500,000*. Swisstopo: Bundesamt für Landestopografie.
- Borchers, B., Marrero, S., Balco, G., Caffee, M., Goehring, B., Lifton, N., et al. (2016). Geological calibration of spallation production rates in the CRONUS-Earth project. *Quaternary Geochronology*, 31, 188–198.
- Christl, M., Vockenhuber, C., Kubik, P. W., Wacker, L., Lachner, J., Alfimov, V., et al. (2013). The ETH Zurich AMS facilities: performance parameters and reference materials. *Nuclear Instruments and Methods in Physics Research, Section B: Beam Interactions with Materials and Atoms*, 294, 29–38.
- Corbett, L. B., Bierman, P. R., Graly, J. A., Neumann, T. A., & Rood, D. H. (2013). Constraining landscape history and glacial erosivity using paired cosmogenic nuclides in Upernavik, northwest Greenland. *Geological Society of America Bulletin*, 125, 1539–1553.
- Dunai, T. J., Binnie, S. A., Hein, A. S., & Paling, S. M. (2014). The effects of a hydrogen-rich ground cover on cosmogenic thermal neutrons: Implications for exposure dating. *Quaternary Geochronology*, 22, 183–191.
- Evans, J. M., Stone, J. O. H., Fifield, L. K., & Cresswell, R. G. (1997). Cosmogenic chlorine-36 production in K-feldspar. *Nuclear Instruments and Methods in Physics Research Section B: Beam Interactions with Materials and Atoms*, 123, 334–340.
- Fabel, D., Harbor, J., Dahms, D., James, A., Elmore, D., Horn, L., et al. (2004). Spatial patterns of glacial erosion at a valley scale derived from terrestrial cosmogenic ^{10}Be and ^{26}Al concentrations in rock. *Annals of the Association of American Geographers*, 94, 241–255.
- Fabryka-Martin, J. T. (1988). Production of radionuclides in the earth and their hydrogeologic significance, with emphasis on chlorine-36 and iodine-129. *Ph.D. dissertation*, University of Arizona, Tucson, USA.
- Fahrni, S. M., Wacker, L., Synal, H. A., & Szidat, S. (2013). Improving a gas ion source for ^{14}C AMS. *Nuclear Instruments and Methods in Physics Research, Section B: Beam Interactions with Materials and Atoms*, 294, 320–327.
- Florineth, D., & Schlüchter, C. (1998). Reconstructing the Last Glacial Maximum (LGM) ice surface geometry and flowlines in the Central Swiss Alps. *Eclogae Geologicae Helveticae*, 91, 391–407.
- Goehring, B. M., Schaefer, J. M., Schlüchter, C., Lifton, N. A., Finkel, R. C., Jull, A. J. T., et al. (2011). The Rhone Glacier was smaller than today for most of the Holocene. *Geology*, 39, 679–682.
- Gosse, J. C., & Phillips, F. M. (2001). Terrestrial in situ cosmogenic nuclides: Theory and application. *Quaternary Science Reviews*, 20, 1475–1560.
- Heisinger, B., Lal, D., Jull, A. J. T., Kubik, P., Ivy-Ochs, S., Knie, K., et al. (2002a). Production of selected cosmogenic radionuclides by muons: 2. Capture of negative muons. *Earth and Planetary Science Letters*, 200, 357–369.
- Heisinger, B., Lal, D., Jull, A. J. T., Kubik, P., Ivy-Ochs, S., Neumaier, S., et al. (2002b). Production of selected cosmogenic radionuclides by muons: 1. Fast muons. *Earth and Planetary Science Letters*, 200, 345–355.
- Hippe, K., Ivy-Ochs, S., Kober, F., Zasadni, J., Wieler, R., Wacker, L., et al. (2014). Chronology of Lateglacial ice flow reorganization and deglaciation in the Gotthard Pass area, Central Swiss Alps, based on cosmogenic ^{10}Be and in situ ^{14}C . *Quaternary Geochronology*, 19, 14–26.
- Hippe, K., Kober, F., Baur, H., Ruff, M., Wacker, L., & Wieler, R. (2009). The current performance of the in situ ^{14}C extraction line at ETH. *Quaternary Geochronology*, 4, 493–500.
- Hippe, K., Kober, F., Wacker, L., Fahrni, S. M., Ivy-Ochs, S., Akçar, N., et al. (2013). An update on in situ cosmogenic ^{14}C analysis at

- ETH Zürich. *Nuclear Instruments and Methods in Physics Research, Section B: Beam Interactions with Materials and Atoms*, 294, 81–86.
- Hippe, K., Kober, F., Zeilinger, G., Ivy-Ochs, S., Maden, C., Wacker, L., et al. (2012). Quantifying denudation rates and sediment storage on the eastern Altiplano, Bolivia, using cosmogenic ^{10}Be , ^{26}Al , and in situ ^{14}C . *Geomorphology*, 179, 58–70.
- Holzhauser, H., Magny, M., & Zumbühl, H. J. (2005). Glacier and lake-level variations in west-central Europe over the last 3500 years. *The Holocene*, 15, 789–801.
- Ivy-Ochs, S. (1996). The dating of rock surfaces using in situ produced ^{10}Be , ^{26}Al and ^{36}Cl , with examples from Antarctica and the Swiss Alps. *PhD thesis*, ETH Zürich, Switzerland, 196.
- Ivy-Ochs, S., Kerschner, H., Kubik, P. W., & Schlüchter, C. (2006). Glacier response in the European Alps to Heinrich Event 1 cooling: the Gschnitz stadial. *Journal of Quaternary Science*, 21, 115–130.
- Ivy-Ochs, S., Kerschner, H., Maisch, M., Christl, M., Kubik, P. W., & Schlüchter, C. (2009). Latest Pleistocene and Holocene glacier variations in the European Alps. *Quaternary Science Reviews*, 28, 2137–2149.
- Ivy-Ochs, S., Kerschner, H., & Schlüchter, C. (2007). Cosmogenic nuclides and the dating of Lateglacial and Early Holocene glacier variations: The Alpine perspective. *Quaternary International*, 164–165, 53–63.
- Ivy-Ochs, S., & Kober, F. (2008). Surface exposure dating with cosmogenic nuclides. *Quaternary Science Journal*, 57, 157–189.
- Ivy-Ochs, S., Schaefer, J., Kubik, P., Synal, H. A., & Schlüchter, C. (2004). Timing of deglaciation on the northern Alpine foreland (Switzerland). *Eclogae Geologicae Helvetiae*, 97, 47–55.
- Ivy-Ochs, S., Schlüchter, C., Kubik, P. W., Dittrich-Hannen, B., & Beer, J. (1995). Minimum ^{10}Be exposure ages of early Pliocene for the Table Mountain plateau and the Sirius Group at Mount Fleming, Dry Valleys, Antarctica. *Geology*, 23, 1007–1010.
- Joerin, U. E., Stocker, T. F., & Schlüchter, C. (2006). Multicentury glacier fluctuations in the Swiss Alps during the Holocene. *The Holocene*, 16, 697–704.
- Kämpfer, C. (2012). Die neuen Seen: Gletscherseen und deren Ausbrüche am Gruebengletscher (BE) im geologischen Kontext. *M.Sc. thesis*, University of Bern, Switzerland, 75.
- Kämpfer, C., & Hählen, N. (2014). Gruebengletscher Guttannen—Spurensuche in Gelände und Archiven zu den Gletscherseeausbrüchen. *Mitteilungen der Naturforschenden Gesellschaft in Bern*, 73–94.
- Kohl, C. P., & Nishiizumi, K. (1992). Chemical isolation of quartz for measurement of in situ-produced cosmogenic nuclides. *Geochimica et Cosmochimica Acta*, 56, 3583–3587.
- Kubik, P. W., & Christl, M. (2010). ^{10}Be and ^{26}Al measurements at the Zurich 6MV Tandem AMS facility. *Nuclear Instruments and Methods in Physics Research, Section B: Beam Interactions with Materials and Atoms*, 268, 880–883.
- Lal, D. (1991). Cosmic ray labeling of erosion surfaces: In situ nuclide production rates and erosion models. *Earth and Planetary Science Letters*, 104, 424–439.
- Lifton, N. A., Jull, A. J. T., & Quade, J. (2001). A new extraction technique and production rate estimate for in situ cosmogenic ^{14}C in quartz. *Geochimica et Cosmochimica Acta*, 65, 1953–1969.
- Maisch, M., Wipf, A., Denzler, B., Battaglia, J., & Benz, C. (1999). *Die Gletscher der Schweizer Alpen. Gletscherhochstand 1850, Aktuelle Vergletscherung, Gletscherschwund-Szenarien*. vdf Hochschulverlag ETH Zürich.
- Marrero, S. M., Phillips, F. M., Caffee, M. W., & Gosse, J. C. (2016). CRONUS-Earth cosmogenic ^{36}Cl calibration. *Quaternary Geochronology*, 31, 199–219.
- Miller, G. H., Briner, J. P., Lifton, N. A., & Finkel, R. C. (2006). Limited ice-sheet erosion and complex exposure histories derived from in situ cosmogenic ^{10}Be , ^{26}Al , and ^{14}C on Baffin Island, Arctic Canada. *Quaternary Geochronology*, 1, 74–85.
- Nishiizumi, K., Imamura, M., Caffee, M. W., Southon, J. R., Finkel, R. C., & McAninch, J. (2007). Absolute calibration of ^{10}Be AMS standards. *Nuclear Instruments and Methods in Physics Research, Section B: Beam Interactions with Materials and Atoms*, 258, 403–413.
- Phillips, F. M., Stone, W. D., & Fabryka-Martin, J. T. (2001). An improved approach to calculating low-energy cosmic-ray neutron fluxes near the land/atmosphere interface. *Chemical Geology*, 175, 689–701.
- Schimmelpfennig, I., Schaefer, J. M., Akcar, N., Koffman, T., Ivy-Ochs, S., Schwartz, R., et al. (2014). A chronology of Holocene and Little Ice Age glacier culminations of the Steingletscher, Central Alps, Switzerland, based on high-sensitivity beryllium-10 moraine dating. *Earth and Planetary Science Letters*, 393, 220–230.
- Stone, J. O. (2000). Air pressure and cosmogenic isotope production. *Journal of Geophysical Research: Solid Earth*, 105, 23753–23759.
- Stone, J. O., Allan, G. L., Fifield, L. K., & Cresswell, R. G. (1996). Cosmogenic chlorine-36 from calcium spallation. *Geochimica et Cosmochimica Acta*, 60, 679–692.
- Swisstopo. (1865). Topographische Karte der Schweiz (Dufourkarte), Bundesamt für Landestopografie.
- Wacker, L., Fahrni, S., Hajdas, I., Molnar, M., Synal, A., Szidat, S., et al. (2013). A versatile gas interface for routine radiocarbon analysis with a gas ion source. *Nuclear Instruments and Methods in Physics Research B*, 294, 315–319.
- Wirsig, C., Zasadni, J., Ivy-Ochs, S., Christl, M., Kober, F., & Schlüchter, C. (2016). A deglaciation model of the Oberhasli, Switzerland. *Journal of Quaternary Science*, 31, 46–59.
- Young, N. E., Schaefer, J., Goehring, B. M., Lifton, N., Schimmelpfennig, I., & Briner, J. (2014). West Greenland and global in situ ^{14}C production-rate calibrations. *Journal of Quaternary Science*, 29, 401–406.
- Zreda, M. (1994). *Development and calibration of the ^{36}Cl surface exposure dating method and its application to the chronology of Late Quaternary glaciations*. New Mexico Institute of Mining and Technology.